The Golgi complex is a regulatory hub for homologous recombination-mediated DNA repair.

George Galea[1*], Karolina Kuodyte[1,2], Muzamil M. Khan[1,3], Peter Thul[4], Beate Neumann[5], Emma Lundberg[4,6,7], Rainer Pepperkok[1,3,5*]

[1]Cell Biology and Biophysics Unit, European Molecular Biology Laboratory (EMBL), 69117 Heidelberg, Germany
[2]Collaboration for joint PhD degree between EMBL and Heidelberg University, Faculty of Biosciences
[3]Translational Lung Research Center Heidelberg, German Center for Lung Research, Heidelberg, Germany
[4]Science for Life Laboratory, School of Engineering Sciences in Chemistry, Biotechnology and Health, KTH - Royal Institute of Technology, Stockholm, 17121, Sweden.
[5]Advanced Light Microscopy Facility, EMBL, Heidelberg, 69117, Heidelberg, Germany
[6]Department of Bioengineering, Stanford University, Stanford, CA 94305, USA
[7]Department of Pathology, Stanford University, Stanford, CA 94305, USA

*corresponding authors
e-mail: george.galea@embl.de; rainer.pepperkok@embl.org

Abstract

Cells are constantly exposed to a multitude of DNA damaging agents that can lead to mutation, dysregulation, and possibly cell death. To ensure genomic integrity, DNA Damage Response (DDR) mechanisms are set in motion to repair and mitigate any damage to the DNA structure. Although these pathways are well-studied in the context of nuclear function, relatively little is known of the regulatory function of cytoplasmic organelles. Here we show the first example of DDR regulation at the Golgi complex, coordinating Homologous Recombination (HR)-mediated DNA repair. We found that RAD51C, a regulatory HR protein, localises to the Golgi and nuclear compartments and in response to double-strand DNA breaks, the Golgi protein population of RAD51C redistributes to form nuclear foci. Furthermore, we found that the Golgi localisation of RAD51C is dependent on the Golgin Giantin. Depletion of Giantin induces the redistribution of the RAD51C Golgi pool to form nuclear foci, independent of DNA damage induction, and concurrent with a significant increase in genomic instability and inhibition of HR signalling regulators. This study presents evidence for a novel pathway where the Golgi is a central regulatory hub for HR DDR and potentially other repair pathways, a finding with important therapeutic implications.

Introduction

DNA damage response (DDR) is extensively studied and its many pivotal roles in preservation of genomic integrity such as DNA damage sensing, repair, cell cycle arrest and apoptosis regulation are relatively well-characterised (Chatterjee & Walker, 2017; Ciccia & Elledge, 2010). However, most of this research has exclusively focused on nuclear events, while cytoplasmic organelles' response and regulatory function have only begun to be elucidated. Nevertheless, a few studies have hinted at a link between cytoplasmic organelles, genomic stability and, in turn, cancer, with the Golgi complex emerging as a central theme (Kulkarni-Gosavi et al., 2019; Petrosyan, 2015; Zhang, 2021). The Golgi is an important homeostasis hub, where a multitude of signalling pathways and essential cellular processes intersect (Makhoul et al., 2018; Wilson et al., 2011). Therefore, it is not unexpected that perturbations to the genome would impact the Golgi complex. At a structural level, the Golgi undergoes dramatic morphological changes after the induction of DNA lesions, from ribbon-like perinuclear stack to dispersed fragments (Farber-Katz et al., 2014). A response requiring the phosphorylation of the Golgi oncoprotein Golgi phosphoprotein 3 (GOLPH3) by DDR regulator DNA-dependent protein kinase (DNA-PK). The Golgi dispersion leads to changes in trafficking patterns and is associated with cell survival, although our understanding of this process is still limited (Farber-Katz et al., 2014). Golgi morphology alterations are also a common feature across a wide variety of cancer types and are often reflected in changes in the distribution of Golgi resident proteins (Petrosyan, 2015; Zhang, 2021). Rearrangement of Golgi glycosyltransferases distribution is not uncommon in cancer cells, resulting in defective glycosylation, a process thought to promote cancer development (Bui et al., 2021; Petrosyan, 2015; Zhang, 2021). It remains unclear what the impacts of these Golgi organisational changes are and whether they're part of a response to DNA damage or a cause of carcinogenesis. Further studies are needed to identify the linking pathways that coordinate DDR and Golgi-associated molecular pathways, such as cell cycle progression, apoptosis and membrane trafficking, that ensure cellular homeostasis is maintained during DNA damage.

In an effort to understand the impact of the Golgi complex on DDR, we investigated the regulation of homologous recombination (HR)-mediated DNA repair through the activity of RAD51C. The protein is part of the RAD51 recombinase protein family, which is a key active complex in the recombination-mediated repair of double-strand DNA breaks (Rein et al., 2021; Sullivan & Bernstein, 2018). RAD51C along with the other RAD51 paralogs assemble into subcomplexes aiding in the regulation of RAD51 activity, although the precise cellular function of these paralogs and recruitment mechanisms remain unclear (Sullivan & Bernstein, 2018). RAD51C is required for DDR signalling through the activation of the checkpoint kinase CHK2 and cell cycle arrest in response to DNA damage and it has been postulated that it can regulate the recruitment and translocation of the HR complex via its nuclear localization signal (Badie et al., 2009; French et al., 2003; Gildemeister et al., 2009). The correct functioning of this protein is crucial for the regulation of HR, with mutations in this gene leading to Fanconi anaemia-like syndrome (chromosomal-instability disorder associated with a variety of developmental abnormalities, bone marrow failure and predisposition to leukaemia and other cancers) and high susceptibility to ovarian and breast cancer (Clague et al., 2011; Loveday et al., 2012; Somyajit et al., 2010; Vaz et al., 2010).

Here, we show the first example of a mechanistic model (**Fig. 1a**) for DDR regulation at the Golgi complex, activating HR-mediated DNA repair through the interaction of RAD51C and Giantin. We find that RAD51C, a regulatory HR protein, localises to the Golgi and nuclear compartments and in response to double-strand DNA breaks, the RAD51C Golgi population redistributes to form nuclear foci. This response requires importin-beta mediated nuclear import and the phosphorylation of ATM protein kinase. We further show that the RAD51C Golgi localisation is dependent on the transmembrane Golgi protein, Giantin (GOLGB1). Depletion of Giantin induces the redistribution of the RAD51C Golgi population to form nuclear foci, independent of DNA damage induction. This resulted in a significant increase in genomic instability concurrently with DNA damage response signalling inhibition. Thus, we identify a novel regulatory pathway for the timely control and activation of HR DNA repair at the Golgi complex following DNA damage. We postulate that this novel Golgi-DDR pathway could extend to other types of DNA repair mechanisms as we validate the localisation of 15 other Golgi-localising DDR proteins associated with the diverse DNA repair processes.

Results

RAD51C Golgi population redistributes to the nucleus in response to DNA damage events.

To examine the role of the Golgi complex in homologous recombination (HR)-mediated DNA repair, we examined the role of the HR regulatory repair protein, RAD51C. We began by examining the localisation of the protein using immunofluorescence staining in standard model cell lines, cervical carcinoma HeLa Kyoto (HK) cells, human bone osteosarcoma epithelial cells, U-2 OS and RAD51C high-expressing, human mammary gland epithelial adenocarcinoma cell line, MCF7 (**Fig. 1b; Extended Data Fig. 1a**). We observed that endogenous RAD51C protein was present in a juxta-nuclear compact localisation that colocalized with the Golgi marker, GM130 and a diffused nuclear distribution with some foci present (**Fig. 1b**). This localisation pattern was reproduced in all the tested cell lines (**Extended Data Fig. 1a**). The specificity of the antibody was tested by the depletion of RAD51C (**Extended Data Fig. 1b-d**). Next, to biochemically validate the subcellular

localisation of RAD51C, we isolated nuclear, membrane and cytoplasmic fractions from HK protein extracts. Fractions were verified using well-established markers (GM130 for Golgi membranes, Lamin B1 for the nuclear compartment, alpha-tubulin for the cytoplasmic fraction) and probed for RAD51C presence in each compartment (**Fig. 1c**). RAD51C was found to be present in all fractions, in agreement with our immunofluorescence data (**Fig. 1b**).

Since RAD51C has been reported to be recruited to DNA repair foci upon the introduction of Double-Strand DNA Breaks (DSBs) (Badie et al., 2009), we induced the formation of these DNA breaks by treating cells with doxorubicin (DOX) and tested whether the Golgi population of RAD51C responds to DNA damage. Upon the addition of the drug (**Fig. 1d-g**), we observed an overall decrease in RAD51C protein level, with the portion of the RAD51C colocalising with the Golgi marker, GM130, reducing at a higher rate than in the nuclear compartment. The RAD51C diffused nuclear pattern changed into very distinct nuclear foci, with this redistribution getting more pronounced with increasing length of treatment (**Fig. 1d, Golgi fraction marked with yellow arrows**). Analysis of these experiments allowed us to measure the changes in RAD51C levels at both the Golgi (**Fig. 1e**) and the nuclear compartment (**Fig. 1f**), and to calculate a RAD51C Golgi-nuclear distribution ratio (**Fig. 1g**). This ratio allowed us to measure robustly and quantitatively the Golgi-nuclear distribution of RAD51C, despite fluctuations of protein levels due to the treatment. After DOX treatment, the ratio value is reduced with increasing length of time when compared to the control, as normalised to 1; giving the RAD51C distribution Golgi:nuclear ratio: 0.86 at 1 h, 0.52 at 2 h, 0.41 at 3 h and 0.32 at 4 h. These results were further validated by subcellular fractionation (**Extended Data Fig. 1e, f**). Similarly, the total protein level of RAD51C is seen to decrease after 3h treatments, with a much larger reduction in the membrane compartment when compared to the nuclear fraction. In both experiments, the RAD51C distribution ratio is seen to decrease significantly after 3 h DOX treatment to 0.41 and 0.69 for the immunofluorescence and biochemical assay, respectively (**Fig. 1g, Extended Data Fig. 1f).**

To further probe this change in the localisation pattern of RAD51C and identify the mechanism of protein redistribution from one compartment to another, we introduced DSBs using DOX while inhibiting the Importin-β-mediated nuclear import, utilising the small peptide inhibitor Importazole (IPZ) (Soderholm et al., 2011). Cells were treated with DMSO (solvent control) or IPZ for 30 min before treatment with DOX (**Fig. 2a, Golgi fraction marked with yellow arrows**). Treatment with IPZ inhibited the previously described DOX-RAD51C localisation pattern change, instead, the majority of the protein population colocalized with the Golgi marker, GM130, and significant inhibition of RAD51C nuclear foci formation was observed **(Fig. 2a-c)**. Quantification of the images (**Fig. 2b, c**) showed that the combinatory treatment of DOX and IPZ significantly inhibited the RAD51C protein redistribution with a calculated RAD51C distribution ratio of 0.68, while the treatment with DOX only resulted in a ratio of 0.31. A reduction in the overall RAD51C protein level was observed when cells were treated with IPZ only, but there was no significant change in the RAD51C distribution pattern, where the distribution ratio was calculated to be 0.83.

Having established that the RAD51C Golgi population responds to DSB-inducing treatments, we sought to test whether the phosphorylation of DDR kinases mediates this redistribution. The three main kinases that are active in response to DNA damage are ataxia-telangiectasia mutated (ATM), Ataxia telangiectasia and Rad3-related (ATR) and DNA-dependent protein kinase (DNA-PK) (Ciccia & Elledge, 2010). We treated cells with phosphorylation inhibitors

specific for each kinase and analysed RAD51C redistribution after DOX treatment (**Fig. 2d-f**). The combination treatment of DOX with the ATM phosphorylation inhibitor, KU55933 (Hickson et al., 2004) significantly inhibited the redistribution of RAD51C, with most of the protein population still colocalising with the Golgi marker, GM130 and a calculated RAD51C distribution ratio of 0.77. Whereas the combined treatment of DOX with ATR and DNA-PK phosphorylation inhibitor, VE-821 (RAD51C distribution ratio of 0.27) (Fokas et al., 2012) and NU7441 (RAD51C distribution ratio of 0.26) (Tavecchio et al., 2012) respectively, had no apparent impact on the redistribution of RAD51C when compared with cells treated with DOX only (RAD51C distribution ratio of 0.31) (**Fig. 2c, Golgi fraction marked with yellow arrows).** No apparent changes in the RAD51C localisation pattern were observed with the treatment of inhibitors only (**Extended Data Fig. 2**).

To ensure that these observations are a direct result of DSBs and not the drug itself, we next investigated the effects of other DSB-causing drugs (Jekimovs et al., 2014): camptothecin (CPT) (**Extended Data Fig. 3a-c**), etoposide (ETO) (**Extended Data Fig. 3d-f**), and mitomycin C (MMC) (**Extended Data Fig. 3g-i**). All treatments showed a significant change in RAD51C distribution, from the Golgi to the nuclear compartment. Furthermore, treatment with CPT (**Extended Data Fig. 3a**) led to a change in RAD51C distribution in the nuclear compartment, from a diffused distribution to distinct nuclear foci, while the application of ETO and MMC (**Extended Data Fig. 3d, g**) resulted in an increase in RAD51C nuclear population but with no apparent nuclear foci pattern.

RAD51C Golgi localisation is dependent on the Golgin Giantin.

To identify potential Golgi candidates that could act as membrane anchors for RAD51C, we analysed two genome-wide siRNA screens carried out to identify regulators of HR and DDR (**Extended Data Fig. 4a, b**) (Adamson et al., 2012; Paulsen et al., 2009). Analysis of the primary data from these screens highlighted the Golgin protein family as potential candidate, where the knockdown of GMAP210 and Giantin lead to a significant reduction in HR repair rates (Adamson et al., 2012) (**Extended Data Fig 4a**), with the depletion of Giantin also leading to a significant inhibition of H2AX phosphorylation, an important DDR signalling regulator (Paulsen et al., 2009) (**Extended Data Fig 4b**). The Golgin family is composed of predominantly coiled-coil proteins that are anchored to the Golgi membrane by their carboxy terminus and are predicted to adopt an extended conformation that projects into the surrounding cytoplasm. This arrangement is ideal for the capture or tethering of nearby membranes (Witkos & Lowe, 2015) and also could potentially act as a surface that retains DDR proteins. Therefore, we tested whether the localization of RAD51C is dependent on these two Golgins (**Fig. 3a-c**). We transfected HK cells with two siRNA targeting GMAP210 or Giantin and monitored for any changes in RAD51C localization. Depletion of GMAP210 and treatment with a control siRNA had no significant effect on RAD51C distribution whereas the knock-down of the Golgi matrix protein Giantin led to a significant redistribution of RAD51C (**Fig. 3a**). We observed a significant decrease in the colocalization of RAD51C with the Golgi marker (**yellow arrows**), GM130 and a change in protein localisation in the nucleus from a diffused distribution to distinct bright nuclear foci (**white arrows**) (**Fig. 3a**)**.** Quantifications showed a reduction of the RAD51C Golgi population (**Fig. 3b**) with the distribution ratio (**Fig. 3c**) reduced by more than half and the number of RAD51C foci (**Fig. 3d**) increased by more than two-fold upon depletion of Giantin with either siRNAs. While there was no significant difference in either RAD51C Golgi intensity, distribution ratio or foci number (**Fig. 3b-d**)

between the GMAP210-depleted and control cells. In light of these results, we next tested whether RAD51C physically interacts or forms a complex with Giantin by performing an immunoprecipitation (IP) assay (**Fig. 3e**). Here, we immunoprecipitated endogenous Giantin, probed for RAD51C and vice versa (**Fig. 3e;** IP: Giantin and IP: RAD51C). Endogenous Giantin and RAD51C were found to co-immunoprecipitate from HK protein extracts in both conditions.

To gain mechanistic insight into the nature of these RAD51C foci induced by Giantin depletion, we carried out colocalization assays to determine whether these structures contain standard HR markers, phosphorylated H2AX (y-H2AX) (**Fig. 4a**) and phosphorylated ATM (p-ATM) (**Fig. 4b**) under physiological conditions. Both proteins are well established markers for DSB repair sites and are important for the recruitment of the HR repair machinery (Vítor et al., 2020). In cells treated with a control siRNA, we observed that a large proportion of the RAD51C nuclear foci were decorated with either y-H2AX or p-ATM (**Fig. 4a, b**; **colocalising foci are denoted with an arrow**), as previously described in literature (Vítor et al., 2020). RAD51C foci induced by the depletion of Giantin showed significantly lower colocalization with both markers. Analysis of these images (**Fig. 4c, d**) showed that 48.6% and 39.2% of RAD51C foci colocalized with y-H2AX and p-ATM respectively under control conditions, whereas RAD51C foci resulting from the depletion of Giantin were found to colocalise significantly less with both markers, with only 17.2% and 15.2% colocalising with y-H2AX and p-ATM respectively.

Depletion of Giantin leads to genomic instability and inhibition of DDR signalling

Having tested the requirement of Giantin in the recruitment and localisation of RAD51C, we next assessed whether the redistribution of the HR protein by the depletion of Giantin would have any significant impact on the cells' ability to maintain genomic stability and undergo DNA repair. To gauge the status of the cell genome, we applied the comet assay (Møller, 2018) which provides a measure of fragmented genomic DNA, an indicator of genomic stability (**Fig. 5a, b**). Cells treated with DNA damaging agents or having impaired DNA repair pathways would result in distinctive long comet tails, due to significant amounts of fragmented genomic DNA. In contrast, healthy untreated cells would display shorter or no comet tail. In our experiment (**Fig. 5a, b**), we observed that samples treated with siRNAs against Giantin and RAD51C showed significantly longer comet tails when compared to the control siRNA treatment. The depletion of RAD51C resulted in the strongest phenotype but was closely followed by the results obtained by the Giantin knockdown. Quantifications of the comets showed that the knockdown of RAD51C resulted in a 2.5-fold increase in the comet tail length and fluorescence intensity, here quantified as a standard metric known as olive tail moment (Olive et al., 2012). Depletion of Giantin using two different siRNAs (siGiantin#1 and siGiantin#2) resulted in 1.8 and 1.6-fold change in the olive tail moment ratio. Next, we validated this effect on genomic stability by measuring the incidence of micronuclei (denoted with red arrows) (**Fig. 5c, d**). We therefore analysed cell populations depleted of Giantin and RAD51C for their occurrence. Our results highlighted a significantly larger percentage of the cell population displayed micronuclei formation and aberrant nuclear structure after the depletion of Giantin and RAD51C when compared to our control samples. We calculated (**Fig. 5d**) that 5% of the population under control conditions displayed micronuclei when compared with 12.5%, 9% and 10% in cells depleted of RAD51C, and two different siRNAs against Giantin, respectively.

RAD51C is required for DSB repair by HR and therefore its mislocalization due to Giantin depletion might lead to inhibition of this pathway and activation of the alternative repair system, the Non-Homologous End Joining (NHEJ) repair (Brandsma & Gent, 2012). To gain insight into the mechanism by which the redistribution of RAD51C leads to a decrease in genomic stability, cells depleted of Giantin were assessed for their ability to phosphorylate and thereby activate well-characterised regulators of HR and NHEJ repair pathways in response to DNA damage (**Fig. 5e, f**). In our negative control, HK cells treated with DOXO and CPT, we observe increased levels of phosphorylated ATM, CHK2, H2AX (**Fig.5e**) and DNA-PK (**Fig. 5f**) in response to the treatment when compared to our solvent control. Cells depleted of the Golgi protein Giantin when treated with DOXO and CPT showed significantly lower levels of phosphorylation of the tested HR DDR proteins except for the NHEJ regulator, DNA-PK, when compared to our control siRNA (**Fig. 5e, f**). Finally, to assess whether this effect is not a result of cell cycle perturbations, we assessed the cell cycle profile of cells depleted of Giantin (**Fig. 5g**), using Fluorescence Activated Cell Sorting (FACS) analysis, where no significant effects were observed.

Antibody-based analysis identifies a network of DNA damage response proteins at the Golgi complex.

To identify other double-localising proteins, similar to RAD51C, which we postulate would link cytoplasmic functions of the secretory pathway to nuclear events, we shortlisted 329 proteins (339 antibodies) identified by the Human Protein Atlas (HPA) project (Thul et al., 2017) to localise at both Golgi-like membranes and the cell nucleus (**Supplementary table S1**). To confirm the localisation data and validate the specificity of the antibody binding, we measured the changes of antibody staining at the Golgi and nuclear compartment after siRNA-mediated knockdown of the target proteins. Candidate antibodies that displayed a 25% or more decrease in fluorescent intensity in both compartments after depletion were considered to be validated (Stadler et al., 2012) with in total 163 candidates (167 antibodies) validated. (**Supplementary table S1**).

All the validated proteins were interrogated by STRING (Szklarczyk et al., 2021) and Reactome gene enrichment database (Gillespie et al., 2022). Much to the confirmation of our proposed hypothesis, two major protein networks were identified, a membrane trafficking and a DDR cluster (**Fig. 6a**). The latter was found to be composed of 15 proteins that function in various components of the core DNA repair complexes: HR DNA repair: RAD51C & NBN (**Fig. 6b**); Non-Homologous End Joining (NHEJ): POLQ & USP1; Mismatch DNA Repair (MMR): MSH6 (**Fig. 6b**) & Base Excision Repair (BER): LIG1 & TOPORS, as well as other integral regulators of DNA repair cellular response such as chromatin cohesion (ESCO2) (**Fig. 6a, b**), ubiquitination (USP1), cell cycle (CCAR1) and signalling (PFDN6 & FMN2). To our knowledge, these findings present the first validation of DNA repair protein clusters to localise to the Golgi complex.

Discussion

The Golgi complex is a key regulatory hub with numerous cellular processes intersecting at this organelle (Makhoul et al., 2018; Wilson et al., 2011). Therefore, understanding the role of the Golgi in response to DNA damage is crucial for discerning the system-wide mechanism at play for maintaining cellular homeostasis. Here we show a novel regulatory pathway that links

the Golgi complex and its cytoplasmic functions to DDR for the activation of HR-mediated DNA repair. A mechanism driven by the Golgi localisation of RAD51C and its interaction with the Golgin, Giantin. Previous studies have shown that RAD51C is essential for the recombination-mediated repair of DSBs and is recruited to the sites of DNA lesions (Badie et al., 2009; Gildemeister et al., 2009). In line with these findings, we show that the RAD51C Golgi population redistributes and forms nuclear foci in response to the DNA damage via an importin-beta mediated transport. Additionally, we show that Giantin is required to maintain the Golgi localisation of RAD51C and the disruption of this interaction leads to inhibition of HR DNA damage response, resulting in increased genomic instability. Consistent with previous literature (Badie et al., 2009), we found that RAD51C Golgi population redistribution requires ATM activity, although the mechanism of recruitment is still unclear, however, another DDR kinase, DNA-PKcs (Farber-Katz et al., 2014), has been shown to interact with the Golgi complex. It is possible that ATM functions in a similar manner for the recruitment of RAD51C at the Golgi, with Giantin being a possible phosphorylation target as previously predicted (Cara et al., 2016).

Here, we propose a model where the cytoplasmic tail of Giantin anchors RAD51C to the Golgi complex, hiding its nuclear localisation sequence motif (French et al., 2003), which would otherwise facilitate its shuttling from the Golgi to the nucleus. When required RAD51C would be activated by the kinase, ATM and recruited to the DNA damage site, and engage other HR repair proteins or further propagate DDR signalling. Consistent with our hypothesis, we found that the mislocalization of RAD51C by Giantin depletion impairs HR signalling response and results in a significant increase in genomic instability. Previous findings also have shown that the depletion of Giantin inhibited both HR repair rates (Adamson et al., 2012) and phosphorylation of the DDR signalling protein, H2AX (Paulsen et al., 2009). However, we cannot exclude that the downregulation of Giantin has impacts on other nuclear events beyond the redistribution of RAD51C, although none of our data and previous literature would suggest this. Interestingly, other members of the Golgin family have also been reported to alter HR repair rates (Adamson et al., 2012) and phosphorylation of DDR signalling protein, H2AX (Paulsen et al., 2009). Numerous studies have also implicated the role of the Golgins in cancer progression (Baschieri et al., 2015; Bhat et al., 2017; Bui et al., 2021; Ghannoum et al., 2022) and although further studies are required to clarify their role, these observations raise the intriguing possibility that this protein family can be integral for DDR regulation.

Taking in the wide array of novel double-localising proteins identified in our study and their respective roles in important cellular processes such as membrane trafficking, cell cycle and DNA damage response, our results propose a high degree of interconnectivity between the secretory membrane system and nuclear compartment. Although further studies are needed to investigate Golgi-DDR pathway functions, our data strongly suggests that the Golgi localisation of RAD51C is crucial for the correct functioning of DSB repair and it is tempting to speculate that the interaction we find for RAD51C and Giantin could be extrapolated to the other DDR proteins identified from this study and the Golgin protein family. When taking into context the established role of the Golgi as a cellular hub for signalling, transport and post-translational modification (Jackson, 2009; Wilson et al., 2011), it comes to no surprise that this organelle could have a function in DNA damage response. The Golgi has already been shown to be a pivotal link between nuclear and cytoplasmic processes such as cholesterol homeostasis (Brown et al., 2018), trafficking events (Scharaw et al., 2016), and mitosis (Colanzi & Sütterlin, 2013). Considering the proximity of the two organelles, the Golgi's cellular

influence in numerous pathways and unique compact architecture, the Golgi is ideal to connect cytoplasmic processes to DDR.

Taken together, our study presents strong evidence for a novel Golgi regulatory pathway for the coordination of HR-mediated repair through the activity of RAD51C and Giantin. Furthermore, our localisation data also suggests that this regulation is not just restricted to HR DNA repair but could extend to all other types of DNA repair mechanisms such as NHEJ, MMR, and BER. This discovery has the potential to open new scientific fields from different ends and has the potential to significantly change the way we understand DNA repair regulation.

Materials and Methods

Antibodies and chemicals. Several commercially antibodies and chemical were used in the paper, including RAD51C (ab72063, Abcam; 1:500 for immunostaining) & (ab95069, Abcam, 1:2000 for western blotting; 1:500 for immunoprecipitation), GOLGB1/Giantin (AF8159, R&D systems; 1:500 for immunostaining and immunoprecipitation, 1:2000 for western blotting) & (G1/M1, Enzo Life Sciences, 1:500 for immunostaining), GM130 (610822, BD Biosciences, 1:500 for immunostaining, 1:2000 for western blotting), ATM Ser1981 (MA1-2020, Invitrogen; 1:500 for immunostaining; 1:2000 for western blotting), CHK2 pThr68 (PA5-17818, Invitrogen; 1:2000 for western blotting), DNA-PKcs (Ser2056) (PA5-78130, Invitrogen, 1:2000 for western blotting), gamma-H2AX pSer139 (613402, Biolegend; 1:500 for immunostaining, 1:2000 for western blotting), alpha-tubulin (MS-581, Thermo Fisher; 1:10,000 for western blotting) Lamin B1 (ab16048, Abcam; 1:2000 for western blotting) vinculin (ab219649, abcam; 1:2000 for western blotting), doxorubicin (ab120629, Abcam); Importazole (SML0341, Sigma-Aldrich), KU55933 (ATMi, SML1109, Sigma-Aldrich); ve-821 (ATRi, HY-14731; MedChemExpress) NU7441 (DNA-PKi, HY-11006; MedChemExpress), etoposide (ab120227, Abcam), mitomycin C (M7949, Sigma-Aldrich), and campothecin (ab120115, Abcam).

Cell lines, cell culture and siRNA transfection. HeLa Kyoto, U2-O S, MCF7, were cultured in DMEM (Life Technologies) supplemented with 10% FBS (Invitrogen) and 1% L-glutamine (Invitrogen). Cells were checked for mycoplasma contamination by PCR. siRNA transfections were performed with Lipofectamine 2000 (Invitrogen) using SilencerSelect siRNAs (Ambion) according to the manufacturer's instructions. Transfections were carried out for 72 h and the final siRNA concentrations used were 15nM for all siRNAs. Giantin siRNA-1: 5951 & siRNA-2: 5953; GMAP210 siRNA-1: s17811 & siRNA-2: s17812; RAD51C siRNA: s11737.

Drug treatments. Cells were treated 24 h after seeding. For camptothecin, etoposide and mitomycin C experiments, cells were treated for 16 h at a concentration of 0.1 μM, 50μM and 5μM, respectively. After treatment cells were incubated with fresh medium for 2 hours. Doxorubicin was used at a concentration of 40μM for 3 h unless indicated otherwise. For kinase and importin-β inhibitor treatments, cells were pretreated for 30 min with the described inhibitor prior to the addition of doxorubicin. The inhibitors were used at the following concentrations: importazole (20μM), KU55933 (30μM), NU7441 (10μM) and ve-821 (10μM).

Immunofluorescence assay. Cells were fixed with 4% paraformaldehyde in PBS and permeabilized with 0.1% Triton X-100 for 15 min at room temperature, then cells were blocked with 5% bovine serum albumin in 0.05% Triton X-100 for 60 min and incubated with primary

antibodies in blocking buffer at room temperature for 3 h. Following 3 washes with PBS, cells were incubated with fluorescent dye-conjugated secondary antibodies diluted in a blocking buffer for 1 h at room temperature.

Image and data analysis. Confocal microscopy experiments were performed with fixed and immunostained cell samples on a microscope FV3000, Olympus. Z stacks of images covering the entire cell thickness were acquired. All image analysis was performed using Cell Profiler (Carpenter et al., 2006) and Fiji (Schindelin et al., 2012). Briefly, first nuclei were segmented in the Hoechst channel. When appropriate, the Golgi complex was segmented in the Golgi marker channel and using the segmented nuclei as seeds, the two structures were associated. Intensity profiles, morphology features and structuring counting analysis were performed when required using Cell Profiler (Carpenter et al., 2006).

Comet assay. The assay was carried out as previously described (Vodenkova et al., 2020). Briefly, cells were trypsinized, pelletized and resuspended in ice-cold PBS at a concentration of 25×10^4 cells per ml. The cells were resuspended in 2% low melting agarose (Sigma) and spread quickly onto gel bond film (Biozym) covered in 1% agarose (Sigma). Samples were immersed into a lysis buffer (100mM EDTA, 2.5M NaCl, 10mM Tris-HCl and 1% Triton-X100; pH 10) overnight at 4°C. Followed by a wash with ice cold water and run in an electrophoresis chamber (alkaline buffer: 1mM EDTA, 300mM NaOH; pH 13) at 15V, 300mA for 60 min at 4°C. Slides were first washed in a Tris-HCl neutralisation buffer (0.4M; pH 7.5) followed by water, stained with SYBR Gold (Thermo Fisher Scientific) (1:10000) and finally dried. Comets were imaged by automated Olympus Scan^R screening microscope and comet tails scored using OpenComet plugin (Gyori et al., 2014).

Western blotting analysis. HK cells were lysed using RIPA buffer (Thermo Scientific) with complete protease inhibitor cocktail (Roche). SDS-PAGE was performed on pre-cast Tris-Acetate gels followed by transfer to PVDF transfer membrane (Merck Millipore). Proteins were detected using primary antibodies as described followed by incubation with secondary antibodies coupled with HRP (Invitrogen). Detection of protein was performed using Pierce ECL Plus Western Blotting Substrate reagent (Thermo Scientific) and visualised on Azure 280 chemiluminescent imaging system. Subcellular fractionation was performed using a subcellular protein fractionation kit for cultured cells (Thermo scientific) according to the manufacturer's instructions. Fractions were verified using well-established markers (GM130 for Golgi membranes, Lamin B1 for the nuclear compartment, alpha-tubulin for the cytoplasmic fraction) and probed for RAD51C presence in each compartment. The RAD51C membrane:nuclear distribution ratio was calculated by first dividing the RAD51C protein level in each fraction by the protein level of the appropriate control, the resulting membrane (M_{R51C} / M_{GM130}) and nuclear (N_{R51C} / $N_{laminB1}$) ratios were further divided to give the ratio = (M_{R51C} / M_{GM130}) / (N_{R51C} / $N_{laminB1}$). The ratios obtained from the control were normalised to 1 and compared to the treated group.

Immunoprecipitation. HK cells were lysed using a lysis buffer (50mM Hepes, 130mM NaCl, 1mM DTT 1% NP-40) with complete protease inhibitor cocktail (Roche). Cell lysates were centrifuged at 13,000 rpm for 10 mins at 4°C. For immunoprecipitation, the lysates were incubated with the primary antibody described and rotated overnight at 4°C. Next, the lysates were incubated with G-agarose beads (Roche) and rotated for 4 h at 4°C. The samples were

washed with cold lysis buffer and then precipitated proteins were eluted by 2x SDS sample buffer and analysed by Western blotting.

Localisation validation siRNA assay. A custom-designed siRNA library targeting our proteins of interest (Ambion) was designed and prepared in 96-well glass bottom plates (Miltenyi Biotec) using a protocol for solid phase reverse transfection as previously described (Erfle et al., 2008; Stadler et al., 2012). Non-targeting siRNA was used as a negative control. 72 hours after cell seeding, cells were fixed with 4% paraformaldehyde, permeabilized with 0.1% Triton-X100 and immunostained against the HPA antibodies of interest and a Golgi marker, GM130. Hoechst 33342 was used as a nuclear stain. siRNAs and antibodies details are available in **Supplementary table S1**. Images were acquired on a fully automated Molecular Devices IXM with a 10x/0.45 NA P-APO objective. The resulting images were analysed using Cell Profiler software (Carpenter et al., 2006) for quantitative and automated measurements of fluorescence from the antibodies as previously described (Stadler et al., 2012). Briefly, nuclei were segmented in the Hoechst channel, the Golgi complex was segmented in the Golgi marker channel and using the segmented nuclei as seeds, the two structures were associated. Intensity profiles of each compartment were acquired. Reduction of 25% or more of the antibody staining in both Golgi and nuclear compartments was considered as a validation of the antibody specificity (**Supplementary table S1**).

Statistical analysis. All data were obtained from at least three independent experiments if not otherwise stated. Statistical analyses were performed using two tailed t-test for pairwise comparison and one-way analysis of variance (ANOVA) for multiple comparisons on GraphPad Prism 9. Data are expressed as standard error of the mean (s.e.m.). n values indicate biologically independent samples and experiments. $P < 0.05$ was considered statistically significant.

Acknowledgements. We thank the ALMF and the Pepperkok team for their support. In addition, we acknowledge Jan Ellenberg, Claudia Lukas, and Simone Köehler for fruitful discussion for the development of the project and manuscript. G.G. was supported by the EMBL EIPOD programme, K.K. by the EMBL PhD programme and M.M.K. by the German Centre for Lung Research..

Figure legend

Figure 1.* RAD51C localises to both the Golgi and nuclear compartment and *redistributes in response to DNA damage events. (a) Proposed mechanistic model for the regulation of HR-mediated repair through the activation of RAD51C at the Golgi complex. (b) Representative images of HK cells stained with antibodies against RAD51C (green) and GM130 (red). DNA was stained with Hoechst 33342 (blue). (c) Western blot showing the subcellular membrane (M), nuclear (N) and cytoplasmic (C) fractions of RAD51C. (d) HK cells treated with the DNA damage inducing drug, doxorubicin (DOX), for increasing lengths of time. Yellow arrows denote the Golgi membrane; Scale bar 10 µm. (e) Quantification of sum intensity of RAD51C Golgi population, (f) RAD51C nuclear population, and (g) a ratio of RAD51C Golgi-nuclear distribution after treatment with DOX. Data represent the mean ± standard error of the mean (s.e.m.). ($n = 3$ biologically independent samples).

Statistical significance was determined using one-way analysis of variance (ANOVA); *$P < 0.05$; **$P < 0.01$; ***$P < 0.001$; ****$P < 0.001$.

Figure 2. Redistribution of RAD51C Golgi fraction is required for the formation of RAD51C nuclear foci and is dependent on the kinase ATM. HK cells were stained with antibodies against RAD51C and GM130. (a) HK cells were treated with DMSO or IPZ prior to a 3-hour treatment with DOX. Yellow arrows denote the Golgi membrane. Results were quantified as (b) relative sum intensity of RAD51C at the Golgi and (c) ratio of RAD51C Golgi-nuclear distribution. (d) HK cells were treated with DMSO (control) alone or with ATM inhibitor (KU55933) or ATR inhibitor (VE-821) or DNA-PK inhibitor (NU7441) prior to a 3-hour treatment with doxorubicin. Results were quantified as an (e) relative sum intensity of RAD51C at the Golgi and (f) ratio of RAD51C Golgi-nuclear distribution. Scale bar 10 μm. Data represent the mean ± standard error of the mean (s.e.m.). ($n = 3$ biologically independent samples). Statistical significance was determined using one-way analysis of variance (ANOVA); *$P < 0.05$; **$P < 0.01$; ***$P < 0.001$; ****$P < 0.001$.

Figure 3. RAD51C Golgi localization and activation is dependent on the Golgin protein Giantin. (a) HK cells were transfected with control, or Giantin siRNAs for 72 hours. The cells were stained with antibodies against RAD51C and Golgi marker GM130. Yellow arrows indicate the Golgi and white arrows indicate nuclear foci; scale bar 10 μm. Quantification of the localisation changes of RAD51C were quantified as (b) relative sum intensity of RAD51C at the Golgi, (c) fluorescent intensity ratio of the RAD51C Golgi-nuclear distribution and (d) relative number of RAD51C foci per cell. Data represent the mean ± standard error of the mean (s.e.m.). ($n = 3$ biologically independent samples). Statistical significance was determined using one-way ANOVA; *$P < 0.05$; **$P < 0.01$; ***$P < 0.001$; ****$P < 0.001$. (e) Immunoprecipitation of Giantin with RAD51C.

Figure 4. Colocalization analysis of RAD51C nuclear foci induced by Giantin depletion with DDR markers. (a-b) Co-localisation experiment of cells treated with control siRNA, or Giantin siRNA. Cell stain with antibody against RAD51C (green) and HR DDR markers (red): (a) y-H2AX, and (b) p-ATM. Co-localisation of structure is denoted by an arrow; Scale bar 10 μm. (i) Quantification of percentage RAD51C foci co-localising with y-H2AX and p-ATM. Data represent the mean ± standard error of the mean (s.e.m.). ($n = 3$ biologically independent samples). Statistical significance was determined using a two-tailed unpaired Student's *t*-test; *$P < 0.05$.

Figure 5. Depletion of Giantin led to increased genomic instability and disruption of DDR signalling. (a) Representative images of comet assay detection genomic DNA fragmentation in HK cells treated with control, Giantin, or RAD51C targeting siRNA. (b) Quantification of comet OliveMoment. (c, d) Representative images and quantification of percentage cells displaying micronuclei after siRNA treatment; scale bar 10 μm. Red arrows denote micronuclei structures. Data represent the mean ± standard error of the mean (s.e.m.). ($n = 3$ biologically independent samples). Statistical significance was determined using one-way analysis of variance (ANOVA); *$P < 0.05$; **$P < 0.01$; ***$P < 0.001$; ****$P < 0.001$. (e, f) HK cells transfected with control or Giantin siRNAs and treated with doxorubicin or camptothecin after 72 h transfection, the extracts were prepared and immunoblotted as indicated. (g) Cell cycle profile of HK cell treated with Giantin or control siRNA. Data represent the mean ± standard error of the mean (s.e.m.). ($n = 3$ biologically independent samples).

Figure 6. **Antibody-based analysis identifies a network of DNA damage response proteins at the Golgi complex.** (a) Protein-protein interaction network showing the DDR proteins identified to localise to both the Golgi complex and nucleus; yellow nodes indicate double-localising proteins, grey nodes are filler untested proteins; experimentally-based string network. (b) Representative images showcasing the antibody-based localisation of 3 DDR proteins, displaying both nuclear and Golgi localisation. Scale bar 10 μm. Yellow arrows indicate the Golgi compartment.

EXTENDED DATA FIGURE 1*.* (a) Representative images showing U-2 OS and MCF7 cells stained with antibodies against RAD51C (green) and GM130 (red). DNA was stained with Hoechst 33342 (blue). (b) Representative images showing the RAD51C antibody specificity. HK cells are stained with antibodies against RAD51C and GM130; DNA was stained with Hoechst 33342. (c) Quantification of RAD51C sum intensity after RAD51C depletion. Data represent the mean ± standard error of the mean (s.e.m.). ($n = 3$ biologically independent samples). (d) Western blot showing the level of RAD51C protein level, in RAD51C-depleted and control cells. (e) Western blot showing the subcellular localization of RAD51C treated with the DMSO and doxorubicin. (f) Quantification of WB showing a ratio of RAD51C membrane-nuclear distribution. Data represent the mean ± standard error of the mean (s.e.m.). ($n = 2$ biologically independent samples). Statistical significance was determined using a two-tailed unpaired Student's *t*-test; $^{*}P < 0.05$; $^{****}P < 0.001$.

EXTENDED DATA FIGURE 2*.* HK cells were stained with antibodies against RAD51C and GM130. HK cells were treated with DMSO (control) alone or with ATM inhibitor (KU55933) or ATR inhibitor (VE-821) or DNA-PK inhibitor (NU7441); scale bar 10 μm.

EXTENDED DATA FIGURE 3*.* HK cell stained with antibodies against RAD51C and GM130. Cells were treated with (a) Camptothecin (CPT), (d) etoposide (ETO) and (g) mitomycin C (MMC) for 16 h followed by media change for 2 h; scale bar 10 μm. Quantification of RAD51C percentage distribution between the Golgi and nuclear compartment after (b) CPT, (e) ETO and (h) MMC treatments. Quantification of RAD51C percentage distribution between the Golgi and nuclear compartment after (c) CPT, (f) ETO and (i) MMC treatments. treatments. Data represent the mean ± standard error of the mean (s.e.m.). ($n = 3$ biologically independent samples). Statistical significance was determined using a two-tailed unpaired Student's *t*-test; $^{**}P < 0.01$; $^{****}P < 0.001$.

EXTENDED DATA FIGURE 4. (a) siRNA screen data (Adamson *et al*, 2012) showing the relative homologous recombination (HR) repair rate upon systematic knockdown of the Golgin protein family (grey) and HR complex proteins (black). (b) siRNA screen data (Paulsen et al., 2009) showing the relative percent cell population with phosphorylation of H2AX upon systematic knockdown of the Golgins. The datasets are normalised to the negative control set at 1. (c) HK cells were transfected with control, or Giantin siRNAs for 72 hours. The cells were stained with antibodies against Giantin and nuclei stained with Hoechst 33342; scale bar 10 μm.

References

Adamson, B., Smogorzewska, A., Sigoillot, F. D., King, R. W., & Elledge, S. J. (2012). A

genome-wide homologous recombination screen identifies the RNA-binding protein RBMX as a component of the DNA-damage response. *Nature Cell Biology*, *14*(3), 318–328.

Badie, S., Liao, C., Thanasoula, M., Barber, P., Hill, M. A., & Tarsounas, M. (2009). RAD51C facilitates checkpoint signaling by promoting CHK2 phosphorylation. *The Journal of Cell Biology*, *185*(4), 587–600.

Baschieri, F., Uetz-von Allmen, E., Legler, D. F., & Farhan, H. (2015). Loss of GM130 in breast cancer cells and its effects on cell migration, invasion and polarity. *Cell Cycle* , *14*(8), 1139–1147.

Bhat, G., Hothpet, V.-R., Lin, M.-F., & Cheng, P.-W. (2017). Shifted Golgi targeting of glycosyltransferases and α-mannosidase IA from giantin to GM130-GRASP65 results in formation of high mannose N -glycans in aggressive prostate cancer cells. In *Biochimica et Biophysica Acta (BBA) - General Subjects* (Vol. 1861, Issue 11, pp. 2891–2901). https://doi.org/10.1016/j.bbagen.2017.08.006

Brandsma, I., & Gent, D. C. (2012). Pathway choice in DNA double strand break repair: observations of a balancing act. *Genome Integrity*, *3*(1), 9.

Brown, M. S., Radhakrishnan, A., & Goldstein, J. L. (2018). Retrospective on Cholesterol Homeostasis: The Central Role of Scap. *Annual Review of Biochemistry*, *87*, 783–807.

Bui, S., Mejia, I., Díaz, B., & Wang, Y. (2021). Adaptation of the Golgi Apparatus in Cancer Cell Invasion and Metastasis. *Frontiers in Cell and Developmental Biology*, *9*, 806482.

Cara, L., Baitemirova, M., Follis, J., Larios-Sanz, M., & Ribes-Zamora, A. (2016). The ATM- and ATR-related SCD domain is over-represented in proteins involved in nervous system development. In *Scientific Reports* (Vol. 6, Issue 1). https://doi.org/10.1038/srep19050

Carpenter, A. E., Jones, T. R., Lamprecht, M. R., Clarke, C., Kang, I. H., Friman, O., Guertin, D. A., Chang, J. H., Lindquist, R. A., Moffat, J., Golland, P., & Sabatini, D. M. (2006). CellProfiler: image analysis software for identifying and quantifying cell phenotypes. *Genome Biology*, *7*(10), R100.

Chatterjee, N., & Walker, G. C. (2017). Mechanisms of DNA damage, repair, and mutagenesis. *Environmental and Molecular Mutagenesis*. https://onlinelibrary.wiley.com/doi/abs/10.1002/em.22087

Ciccia, A., & Elledge, S. J. (2010). The DNA damage response: making it safe to play with knives. *Molecular Cell*, *40*(2), 179–204.

Clague, J., Wilhoite, G., Adamson, A., Bailis, A., Weitzel, J. N., & Neuhausen, S. L. (2011). RAD51C germline mutations in breast and ovarian cancer cases from high-risk families. *PloS One*, *6*(9), e25632.

Colanzi, A., & Sütterlin, C. (2013). Signaling at the Golgi during mitosis. *Methods in Cell Biology*, *118*, 383–400.

Erfle, H., Neumann, B., Rogers, P., Bulkescher, J., Ellenberg, J., & Pepperkok, R. (2008). Work flow for multiplexing siRNA assays by solid-phase reverse transfection in multiwell plates. *Journal of Biomolecular Screening*, *13*(7), 575–580.

Farber-Katz, S. E., Dippold, H. C., Buschman, M. D., Peterman, M. C., Xing, M., Noakes, C. J., Tat, J., Ng, M. M., Rahajeng, J., Cowan, D. M., Fuchs, G. J., Zhou, H., & Field, S. J. (2014). DNA damage triggers Golgi dispersal via DNA-PK and GOLPH3. *Cell*, *156*(3), 413–427.

Fokas, E., Prevo, R., Pollard, J. R., Reaper, P. M., Charlton, P. A., Cornelissen, B., Vallis, K.

A., Hammond, E. M., Olcina, M. M., Gillies McKenna, W., Muschel, R. J., & Brunner, T. B. (2012). Targeting ATR in vivo using the novel inhibitor VE-822 results in selective sensitization of pancreatic tumors to radiation. In *Cell Death & Disease* (Vol. 3, Issue 12, pp. e441–e441). https://doi.org/10.1038/cddis.2012.181

French, C. A., Tambini, C. E., & Thacker, J. (2003). Identification of functional domains in the RAD51L2 (RAD51C) protein and its requirement for gene conversion. *The Journal of Biological Chemistry*, *278*(46), 45445–45450.

Ghannoum, S., Fantini, D., Zahoor, M., Reiterer, V., Phuyal, S., Netto, W. L., Sørensen, Ø., Iyer, A., Sengupta, D., Prasmickaite, L., Mælandsmo, G. M., Köhn-Luque, A., & Farhan, H. (2022). A combined experimental-computational approach uncovers a role for the Golgi matrix protein Giantin in breast cancer progression. In *bioRxiv* (p. 2022.04.25.489358). https://doi.org/10.1101/2022.04.25.489358

Gildemeister, O. S., Sage, J. M., & Knight, K. L. (2009). Cellular Redistribution of Rad51 in Response to DNA Damage. *The Journal of Biological Chemistry*, *284*(46), 31945–31952.

Gillespie, M., Jassal, B., Stephan, R., Milacic, M., Rothfels, K., Senff-Ribeiro, A., Griss, J., Sevilla, C., Matthews, L., Gong, C., Deng, C., Varusai, T., Ragueneau, E., Haider, Y., May, B., Shamovsky, V., Weiser, J., Brunson, T., Sanati, N., … D'Eustachio, P. (2022). The reactome pathway knowledgebase 2022. *Nucleic Acids Research*, *50*(D1), D687–D692.

Gyori, B. M., Venkatachalam, G., Thiagarajan, P. S., Hsu, D., & Clement, M.-V. (2014). OpenComet: an automated tool for comet assay image analysis. *Redox Biology*, *2*, 457–465.

Hickson, I., Zhao, Y., Richardson, C. J., Green, S. J., Martin, N. M. B., Orr, A. I., Reaper, P. M., Jackson, S. P., Curtin, N. J., & Smith, G. C. M. (2004). Identification and characterization of a novel and specific inhibitor of the ataxia-telangiectasia mutated kinase ATM. *Cancer Research*, *64*(24), 9152–9159.

Jackson, C. L. (2009). Mechanisms of transport through the Golgi complex. *Journal of Cell Science*, *122*(Pt 4), 443–452.

Jekimovs, C., Bolderson, E., Suraweera, A., Adams, M., O'Byrne, K. J., & Richard, D. J. (2014). Chemotherapeutic compounds targeting the DNA double-strand break repair pathways: the good, the bad, and the promising. *Frontiers in Oncology*, *4*, 86.

Kulkarni-Gosavi, P., Makhoul, C., & Gleeson, P. A. (2019). Form and function of the Golgi apparatus: scaffolds, cytoskeleton and signalling. *FEBS Letters*, *593*(17), 2289–2305.

Loveday, C., Turnbull, C., Ruark, E., Xicola, R. M. M., Ramsay, E., Hughes, D., Warren-Perry, M., Snape, K., Breast Cancer Susceptibility Collaboration (UK), Eccles, D., Evans, D. G., Gore, M., Renwick, A., Seal, S., Antoniou, A. C., & Rahman, N. (2012). Germline RAD51C mutations confer susceptibility to ovarian cancer [Review of *Germline RAD51C mutations confer susceptibility to ovarian cancer*]. *Nature Genetics*, *44*(5), 475–476; author reply 476.

Makhoul, C., Gosavi, P., & Gleeson, P. A. (2018). The Golgi architecture and cell sensing. *Biochemical Society Transactions*, *46*(5), 1063–1072.

Møller, P. (2018). The comet assay: ready for 30 more years. *Mutagenesis*, *33*(1), 1–7.

Olive, P. L., Banáth, J. P., & Durand, R. E. (2012). Heterogeneity in Radiation-Induced DNA Damage and Repair in Tumor and Normal Cells Measured Using the "Comet" Assay. In *Radiation Research* (Vol. 178, Issue 2, pp. AV35–AV42). https://doi.org/10.1667/rrav04.1

Paulsen, R. D., Soni, D. V., Wollman, R., Hahn, A. T., Yee, M.-C., Guan, A., Hesley, J. A., Miller, S. C., Cromwell, E. F., Solow-Cordero, D. E., Meyer, T., & Cimprich, K. A. (2009). A

genome-wide siRNA screen reveals diverse cellular processes and pathways that mediate genome stability. *Molecular Cell*, *35*(2), 228–239.

Petrosyan, A. (2015). Onco-Golgi: Is Fragmentation a Gate to Cancer Progression? *Biochemistry & Molecular Biology Journal*, *1*(1). https://doi.org/10.21767/2471-8084.100006

Rein, H. L., Bernstein, K. A., & Baldock, R. A. (2021). RAD51 paralog function in replicative DNA damage and tolerance. *Current Opinion in Genetics & Development*, *71*, 86–91.

Scharaw, S., Iskar, M., Ori, A., Boncompain, G., Laketa, V., Poser, I., Lundberg, E., Perez, F., Beck, M., Bork, P., & Pepperkok, R. (2016). The endosomal transcriptional regulator RNF11 integrates degradation and transport of EGFR. *The Journal of Cell Biology*, *215*(4), 543–558.

Schindelin, J., Arganda-Carreras, I., Frise, E., Kaynig, V., Longair, M., Pietzsch, T., Preibisch, S., Rueden, C., Saalfeld, S., Schmid, B., Tinevez, J.-Y., White, D. J., Hartenstein, V., Eliceiri, K., Tomancak, P., & Cardona, A. (2012). Fiji: an open-source platform for biological-image analysis. *Nature Methods*, *9*(7), 676–682.

Soderholm, J. F., Bird, S. L., Kalab, P., Sampathkumar, Y., Hasegawa, K., Uehara-Bingen, M., Weis, K., & Heald, R. (2011). Importazole, a small molecule inhibitor of the transport receptor importin-β. *ACS Chemical Biology*, *6*(7), 700–708.

Somyajit, K., Subramanya, S., & Nagaraju, G. (2010). RAD51C: a novel cancer susceptibility gene is linked to Fanconi anemia and breast cancer. *Carcinogenesis*, *31*(12), 2031–2038.

Stadler, C., Hjelmare, M., Neumann, B., Jonasson, K., Pepperkok, R., Uhlén, M., & Lundberg, E. (2012). Systematic validation of antibody binding and protein subcellular localization using siRNA and confocal microscopy. *Journal of Proteomics*, *75*(7), 2236–2251.

Sullivan, M. R., & Bernstein, K. A. (2018). RAD-ical New Insights into RAD51 Regulation. *Genes*, *9*(12). https://doi.org/10.3390/genes9120629

Szklarczyk, D., Gable, A. L., Nastou, K. C., Lyon, D., Kirsch, R., Pyysalo, S., Doncheva, N. T., Legeay, M., Fang, T., Bork, P., Jensen, L. J., & von Mering, C. (2021). The STRING database in 2021: customizable protein-protein networks, and functional characterization of user-uploaded gene/measurement sets. *Nucleic Acids Research*, *49*(D1), D605–D612.

Tavecchio, M., Munck, J. M., Cano, C., Newell, D. R., & Curtin, N. J. (2012). Further characterisation of the cellular activity of the DNA-PK inhibitor, NU7441, reveals potential cross-talk with homologous recombination. *Cancer Chemotherapy and Pharmacology*, *69*(1), 155–164.

Thul, P. J., Åkesson, L., Wiking, M., Mahdessian, D., Geladaki, A., Ait Blal, H., Alm, T., Asplund, A., Björk, L., Breckels, L. M., Bäckström, A., Danielsson, F., Fagerberg, L., Fall, J., Gatto, L., Gnann, C., Hober, S., Hjelmare, M., Johansson, F., … Lundberg, E. (2017). A subcellular map of the human proteome. *Science*, *356*(6340). https://doi.org/10.1126/science.aal3321

Vaz, F., Hanenberg, H., Schuster, B., Barker, K., Wiek, C., Erven, V., Neveling, K., Endt, D., Kesterton, I., Autore, F., Fraternali, F., Freund, M., Hartmann, L., Grimwade, D., Roberts, R. G., Schaal, H., Mohammed, S., Rahman, N., Schindler, D., & Mathew, C. G. (2010). Mutation of the RAD51C gene in a Fanconi anemia–like disorder. *Nature Genetics*, *42*(5), 406–409.

Vítor, A. C., Huertas, P., Legube, G., & de Almeida, S. F. (2020). Studying DNA Double-Strand Break Repair: An Ever-Growing Toolbox. *Frontiers in Molecular Biosciences*, *7*, 24.

Vodenkova, S., Azqueta, A., Collins, A., Dusinska, M., Gaivão, I., Møller, P., Opattova, A., Vodicka, P., Godschalk, R. W. L., & Langie, S. A. S. (2020). An optimized comet-based in vitro

DNA repair assay to assess base and nucleotide excision repair activity. *Nature Protocols*, *15*(12), 3844–3878.

Wilson, C., Venditti, R., Rega, L. R., Colanzi, A., D'Angelo, G., & De Matteis, M. A. (2011). The Golgi apparatus: an organelle with multiple complex functions. *Biochemical Journal*, *433*(1), 1–9.

Witkos, T. M., & Lowe, M. (2015). The Golgin Family of Coiled-Coil Tethering Proteins. *Frontiers in Cell and Developmental Biology*, *3*, 86.

Zhang, X. (2021). Alterations of Golgi Structural Proteins and Glycosylation Defects in Cancer. *Frontiers in Cell and Developmental Biology*, *9*, 665289.

FIGURE 1

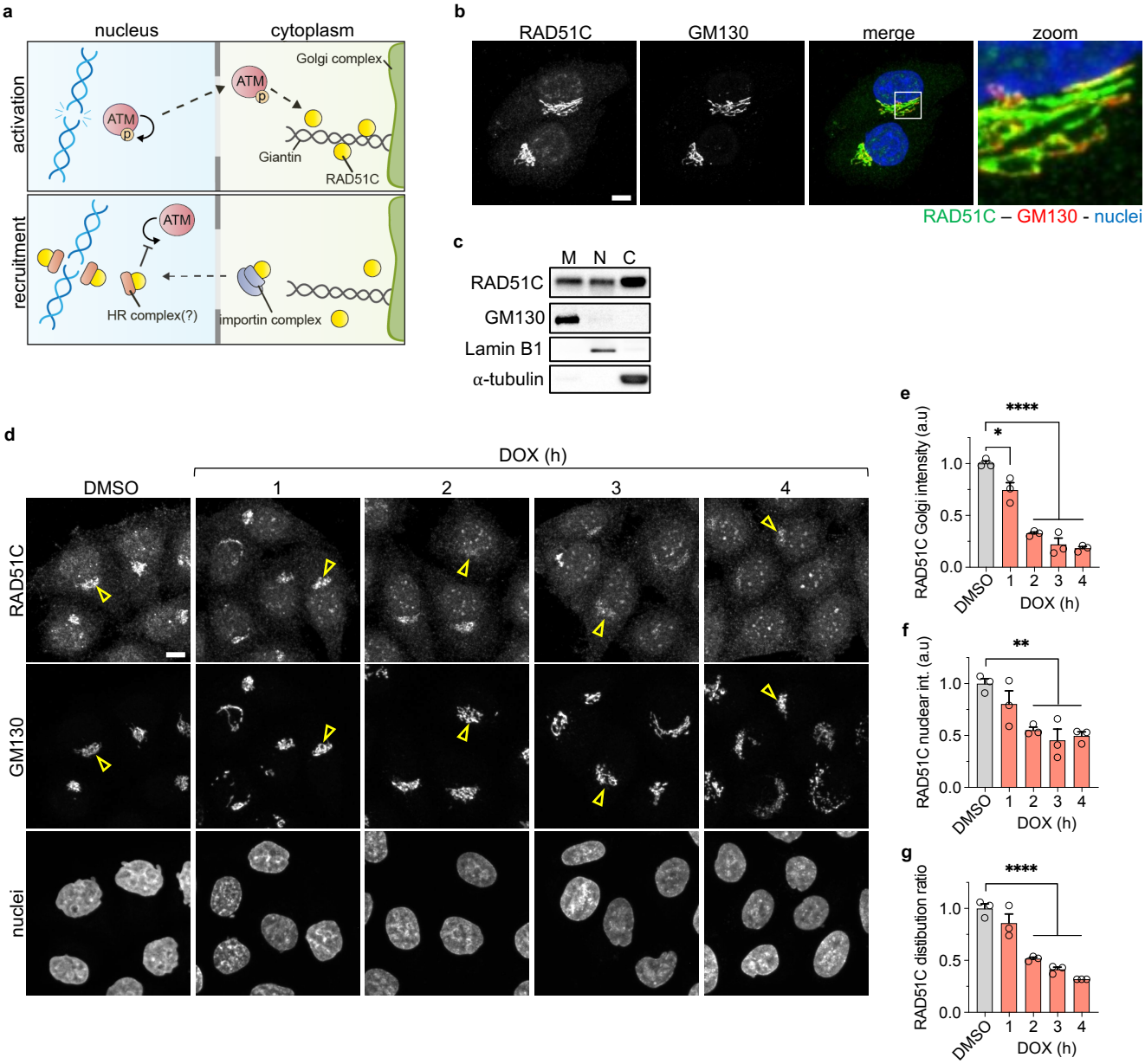
a
nucleus
cytoplasm
activation
recruitment
ATM
p
Golgi complex
Giantin
RAD51C
HR complex(?)
importin complex
b
RAD51C
GM130
merge
zoom
RAD51C – GM130 - nuclei
c
M N C
RAD51C
GM130
Lamin B1
α-tubulin
d
DOX (h)
DMSO
1
2
3
4
RAD51C
GM130
nuclei
e
RAD51C Golgi intensity (a.u)
****
*
1.0
0.5
0.0
DMSO 1 2 3 4
DOX (h)
f
RAD51C nuclear int. (a.u)
**
1.0
0.5
0.0
DMSO 1 2 3 4
DOX (h)
g
RAD51C distibution ratio
****
1.0
0.5
0.0
DMSO 1 2 3 4
DOX (h)

FIGURE 2

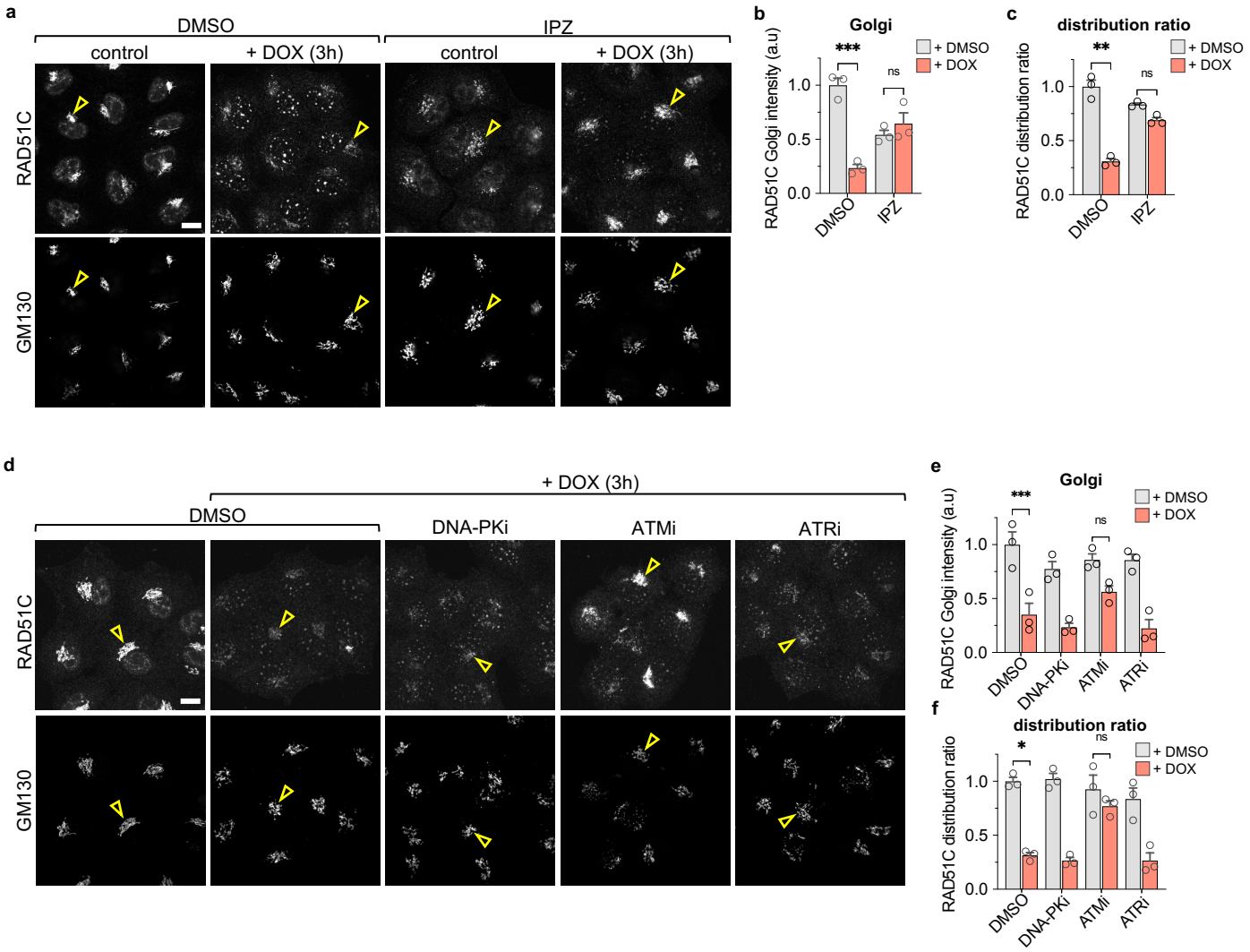
a
DMSO
IPZ
control
+ DOX (3h)
control
+ DOX (3h)
RAD51C
GM130
b
Golgi
RAD51C Golgi intensity (a.u)
***
ns
+ DMSO
+ DOX
1.0
0.5
0.0
DMSO
IPZ
c
distribution ratio
RAD51C distribution ratio
**
ns
+ DMSO
+ DOX
1.0
0.5
0.0
DMSO
IPZ
d
+ DOX (3h)
DMSO
DNA-PKi
ATMi
ATRi
RAD51C
GM130
e
Golgi
RAD51C Golgi intensity (a.u)
***
ns
+ DMSO
+ DOX
1.0
0.5
0.0
DMSO
DNA-PKi
ATMi
ATRi
f
distribution ratio
RAD51C distribution ratio
*
ns
+ DMSO
+ DOX
1.0
0.5
0.0
DMSO
DNA-PKi
ATMi
ATRi

FIGURE 3

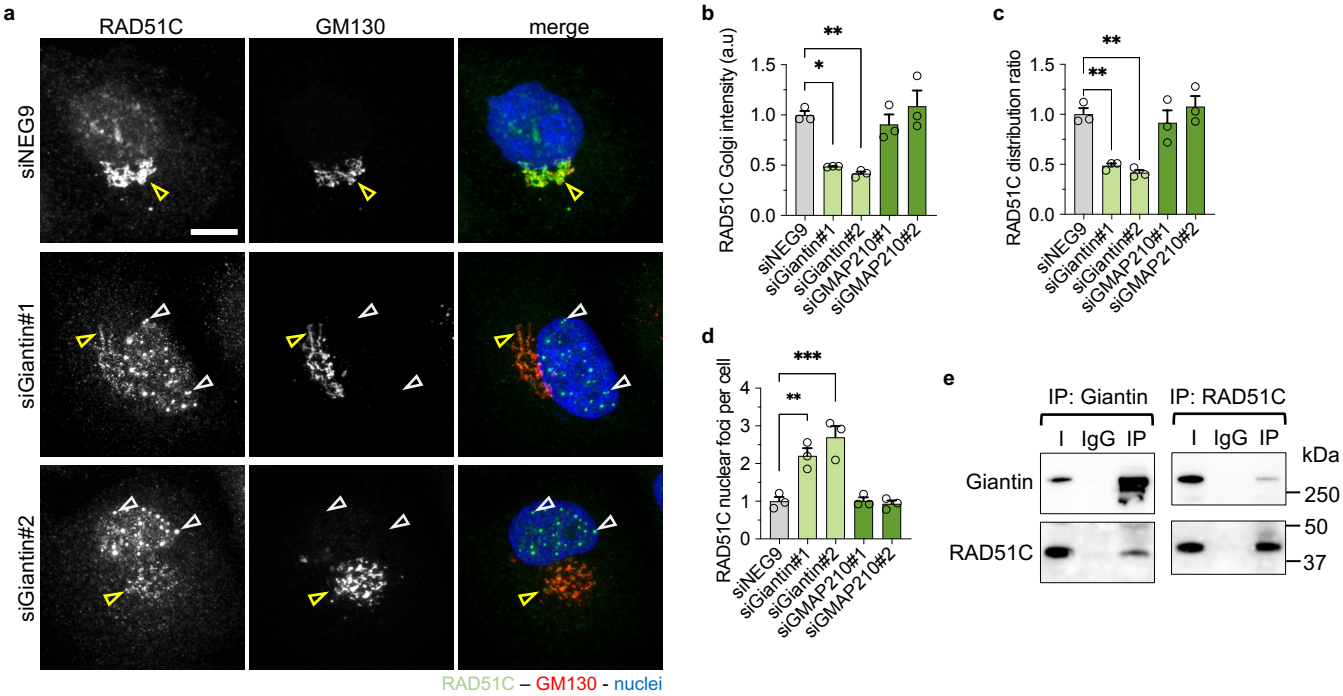
a
RAD51C
GM130
merge
siNEG9
siGiantin#1
siGiantin#2
RAD51C – GM130 - nuclei
b
RAD51C Golgi intensity (a.u)
1.5
1.0
0.5
0.0
*
**
siNEG9
siGiantin#1
siGiantin#2
siGMAP210#1
siGMAP210#2
c
RAD51C distribution ratio
1.5
1.0
0.5
0.0
**
**
siNEG9
siGiantin#1
siGiantin#2
siGMAP210#1
siGMAP210#2
d
RAD51C nuclear foci per cell
4
3
2
1
0
**
***
siNEG9
siGiantin#1
siGiantin#2
siGMAP210#1
siGMAP210#2
e
IP: Giantin
IP: RAD51C
I
IgG
IP
I
IgG
IP
kDa
Giantin
RAD51C
250
50
37

FIGURE 4

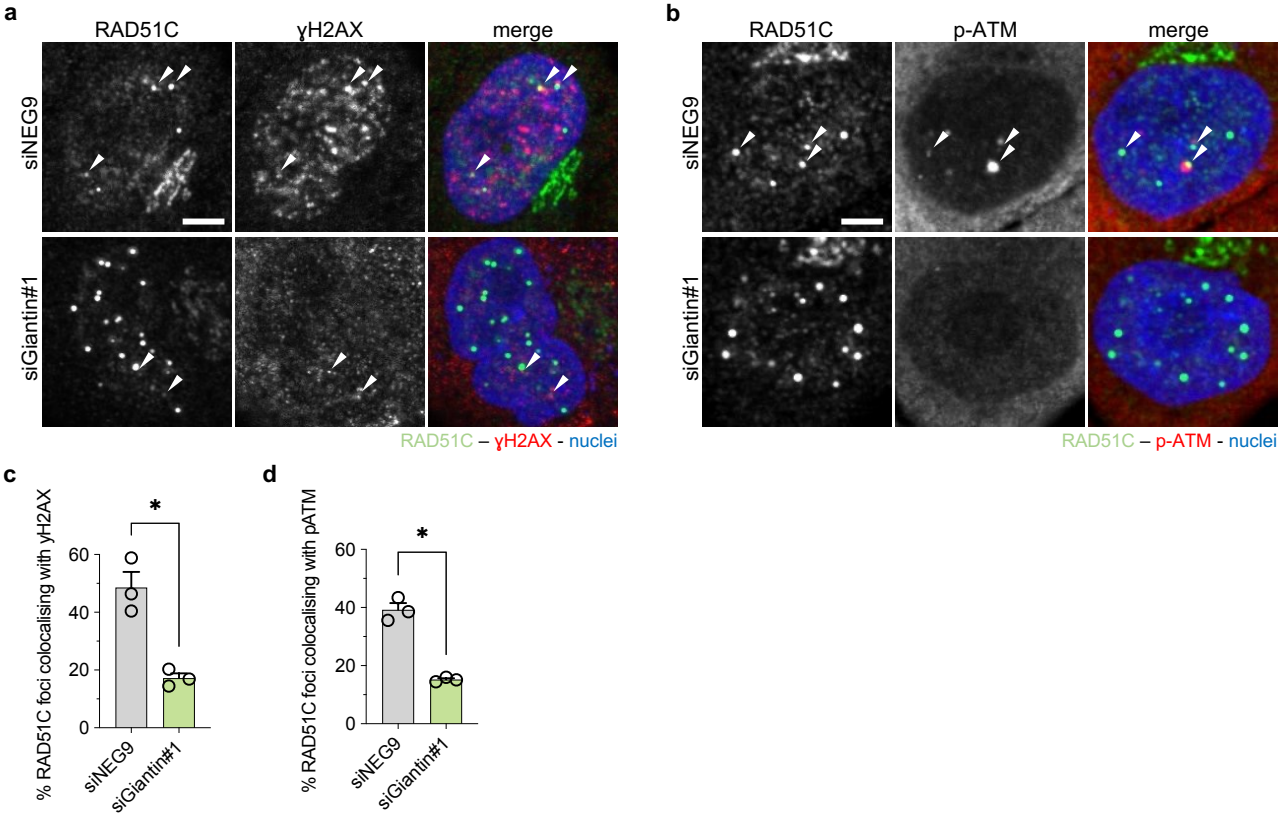
a
RAD51C
γH2AX
merge
siNEG9
siGiantin#1
RAD51C – γH2AX - nuclei
b
RAD51C
p-ATM
merge
siNEG9
siGiantin#1
RAD51C – p-ATM - nuclei
c
% RAD51C foci colocalising with γH2AX
60
40
20
0
*
siNEG9
siGiantin#1
d
% RAD51C foci colocalising with pATM
60
40
20
0
*
siNEG9
siGiantin#1

FIGURE 5

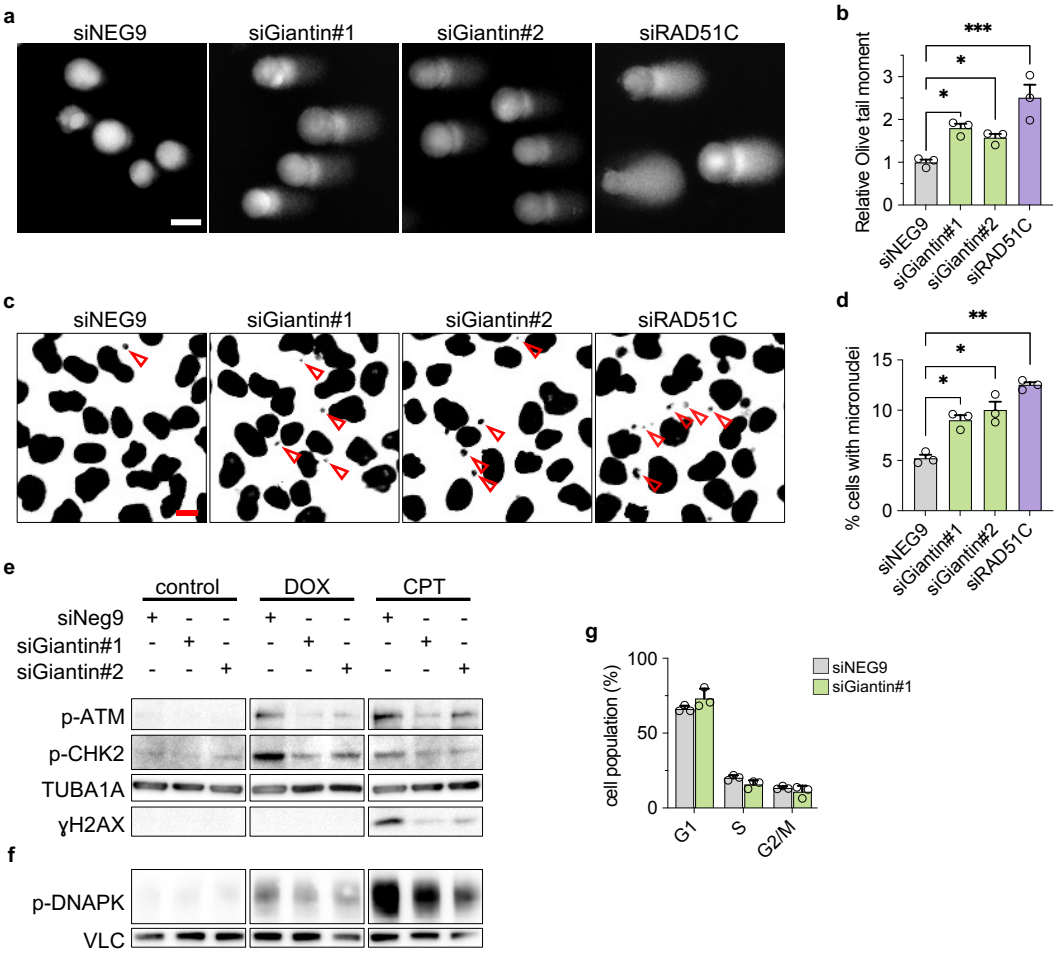
a
siNEG9
siGiantin#1
siGiantin#2
siRAD51C
b
Relative Olive tail moment
***
*
*
0
1
2
3
siNEG9
siGiantin#1
siGiantin#2
siRAD51C
c
siNEG9
siGiantin#1
siGiantin#2
siRAD51C
d
% cells with micronuclei
**
*
*
0
5
10
15
siNEG9
siGiantin#1
siGiantin#2
siRAD51C
e
control
DOX
CPT
siNeg9
siGiantin#1
siGiantin#2
p-ATM
p-CHK2
TUBA1A
γH2AX
f
p-DNAPK
VLC
g
cell population (%)
100
50
0
siNEG9
siGiantin#1
G1
S
G2/M

FIGURE 6

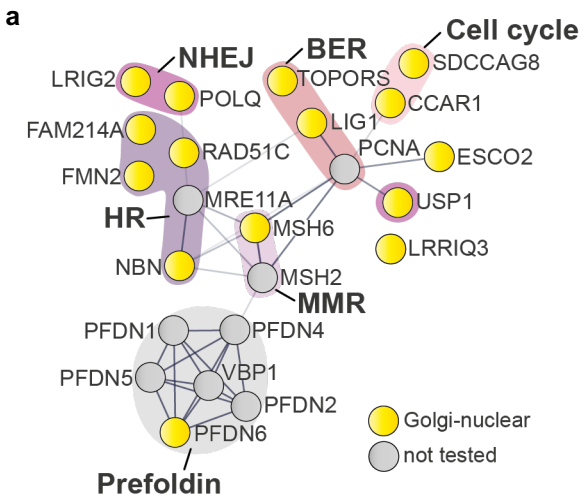
a
NHEJ
BER
Cell cycle
LRIG2
POLQ
TOPORS
SDCCAG8
CCAR1
LIG1
FAM214A
RAD51C
PCNA
ESCO2
FMN2
MRE11A
USP1
HR
MSH6
LRRIQ3
NBN
MSH2
MMR
PFDN1
PFDN4
PFDN5
VBP1
PFDN2
PFDN6
Prefoldin
Golgi-nuclear
not tested

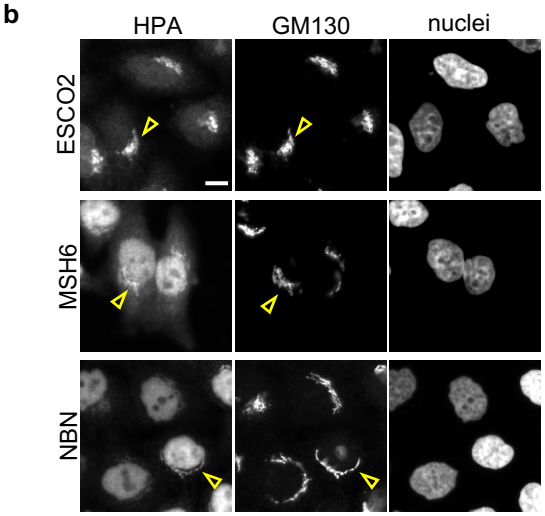
b
HPA
GM130
nuclei
ESCO2
MSH6
NBN

EXTENDED DATA FIGURE 1

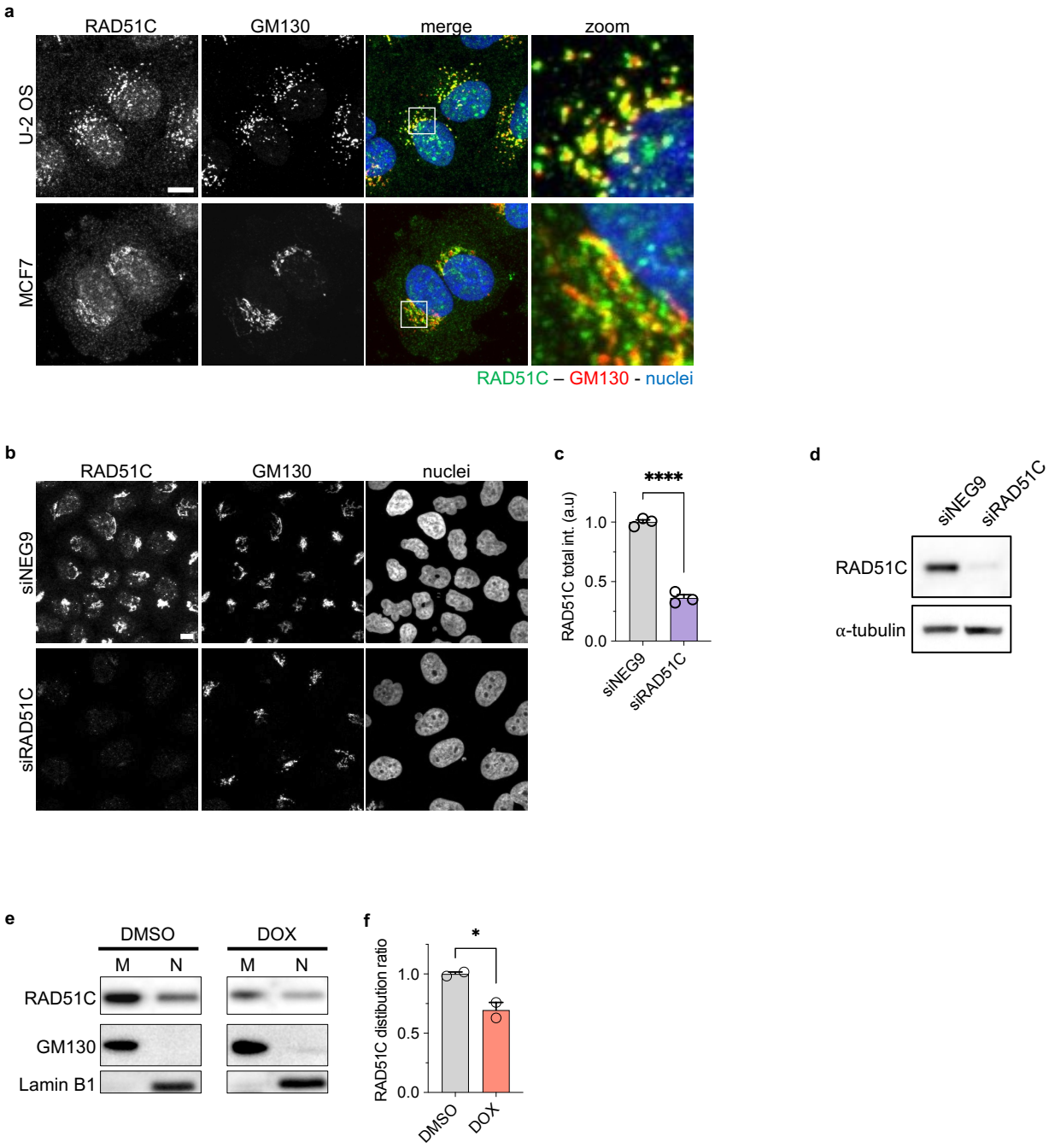

EXTENDED DATA FIGURE 2

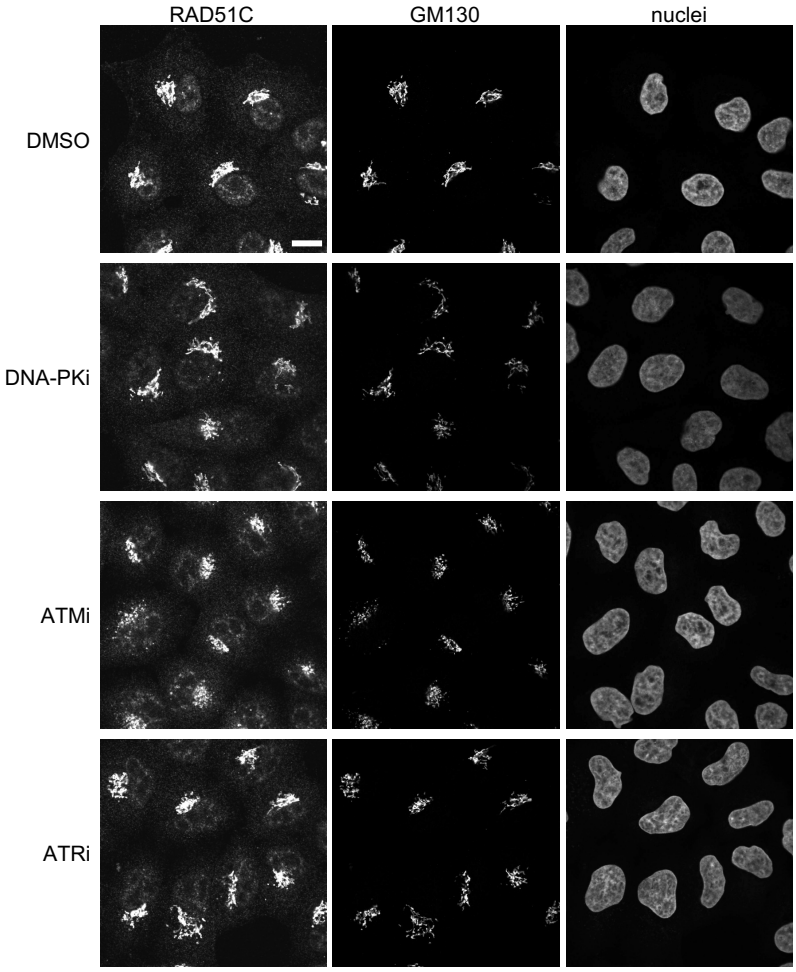

EXTENDED DATA FIGURE 3

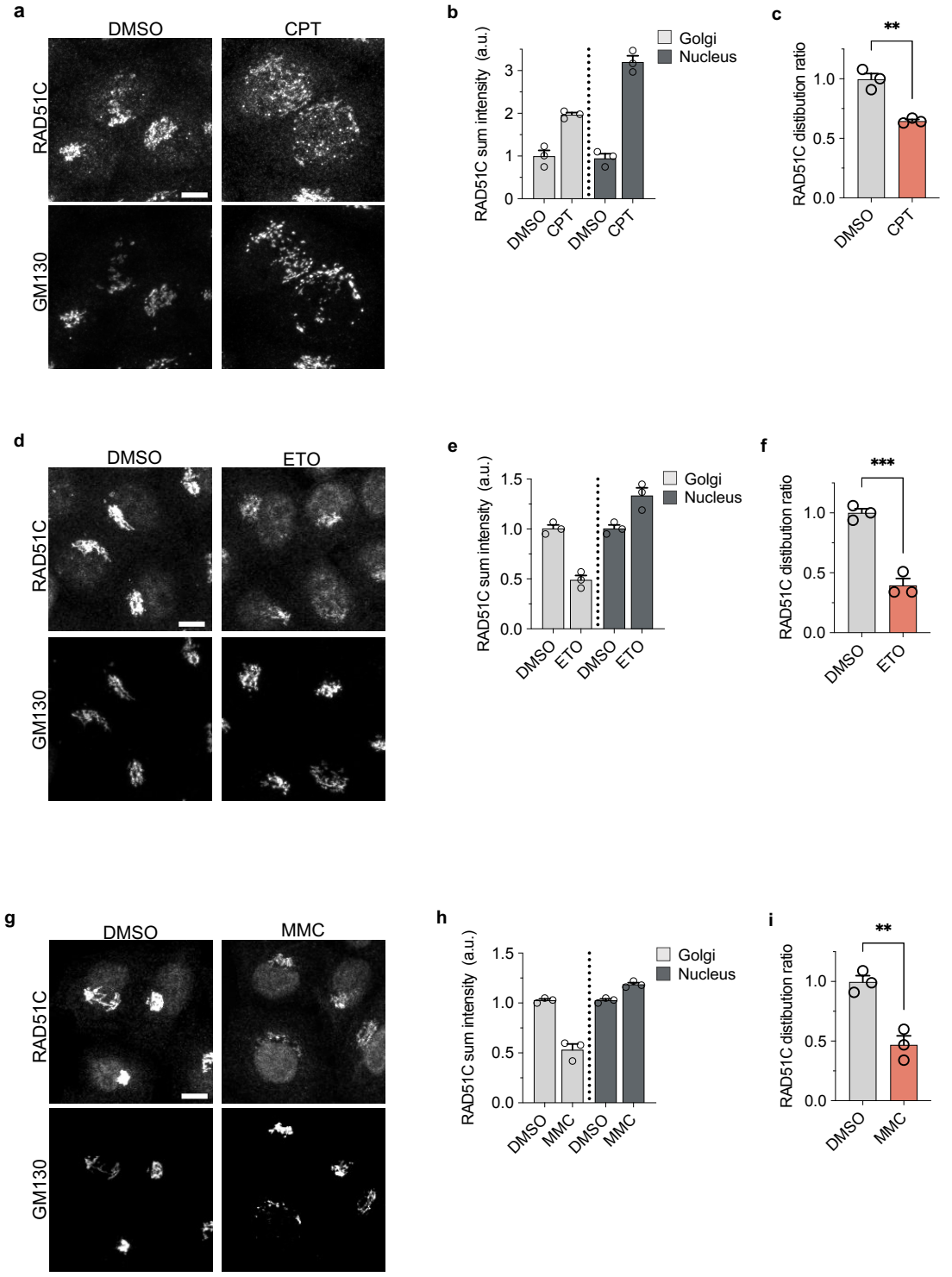
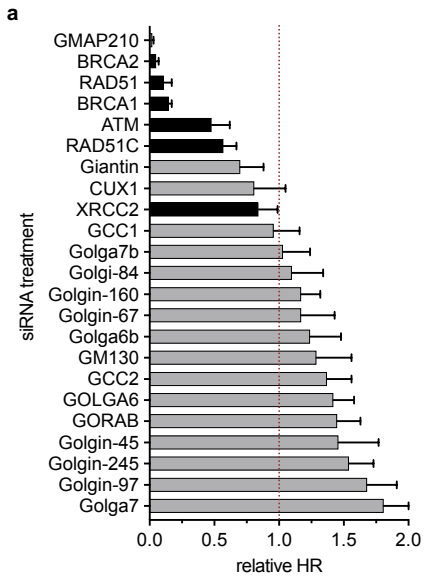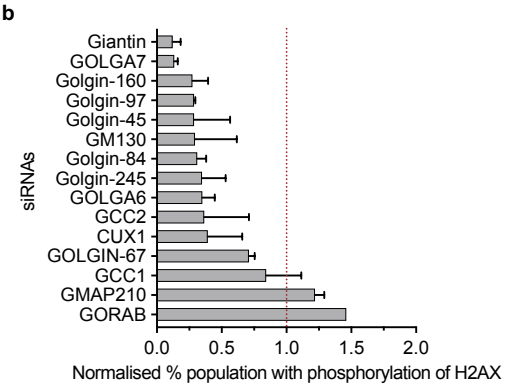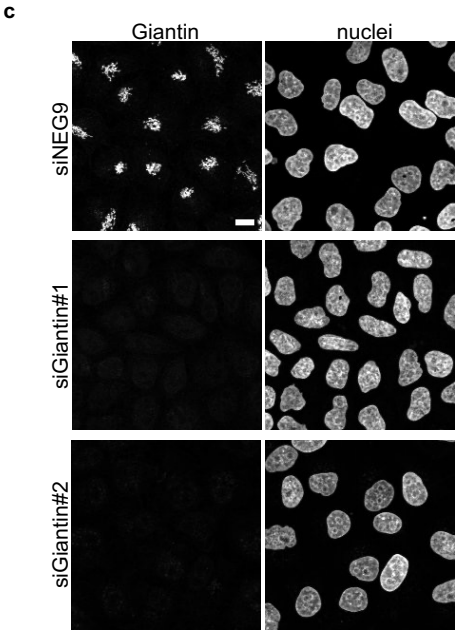
EXTENDED DATA FIGURE 4